Chemical Science

ROYAL SOCIETY OF CHEMISTRY

EDGE ARTICLE

View Article Online
View Journal | View Issue

Cite this: *Chem. Sci.*, 2022, **13**, 6592

All publication charges for this article have been paid for by the Royal Society of Chemistry

Received 10th April 2022
Accepted 15th May 2022

DOI: 10.1039/d2sc02063g

rsc.li/chemical-science

Magnesium-stabilised transition metal formyl complexes: structures, bonding, and ethenediolate formation†

Joseph M. Parr, Andrew J. P. White and Mark R. Crimmin *

Herein we report the first comprehensive series of crystallographically characterised transition metal formyl complexes. In these complexes, the formyl ligand is trapped as part of a chelating structure between a transition metal (Cr, Mn, Fe, Co, Rh, W, and Ir) and a magnesium (Mg) cation. Calculations suggest that this bonding mode results in significant oxycarbene-character of the formyl ligand. Further reaction of a heterometallic Cr–Mg formyl complex results in a rare example of C–C coupling and formation of an ethenediolate complex. DFT calculations support a key role for the formyl-intermediate in ethenediolate formation. These results show that well-defined transition metal formyl complexes are potential intermediates in the homologation of carbon monoxide.

Introduction

Transition metal formyl complexes are important intermediates in the reduction of carbon monoxide (CO) and carbon dioxide (CO_2).[1] For example, transition metal formyl species have been proposed as key intermediates in the reduction of CO with H_2 to form linear alkanes in the Fischer–Tropsch (F–T) process.[2–13] Despite their importance, the detailed study of transition metal formyl complexes has been hampered by their low stability. Early studies established that these species undergo facile α-elimination to form the corresponding hydrido carbonyl complexes.[13–25] The reaction is potentially reversible, but in most cases the hydrido carbonyl is thermodynamically favoured (Scheme 1a).[26–29] Increased oxycarbene character is expected to increase the metal ligand binding energy through strengthening the metal–carbon bond. This then, in turn, should bias the position of the equilibrium toward the metal formyl species rather than the metal hydrido carbonyl complex.[30–33]

A survey of the Cambridge Crystallographic Data Centre (CCDC) database reveals that despite nearly 50 years of research into transition metal formyl complexes, only a modest number have been structurally characterised (supporting information, Fig. S11 and Table S2†). The paucity of data has meant that there is currently no systematic study into the effect of the transition metal on the bonding of structurally characterised formyl complexes.

Due to the challenge in studying transition metal formyl complexes, even the simplest steps involving these intermediates can be ill-defined. Take for example ethenediolate $\{C_2H_2O_2\}^{2-}$ formation from combining two CO and two H^- ligands on a transition metal (Scheme 1b). This type of C–C bond formation is relevant to F–T type chemistry where metal-bound CO and H^- ligands are prevalent.[34–36] Transition metal formyl complexes were originally proposed as intermediates in ethenediolate formation by Bercaw and co-workers.[37] Direct support for their involvement is however limited. Studies in the 1980s, largely relied on the use of more stable metal acyl derivatives to explore the fundamental steps of these ligand types.[38,39] In a single case, Marks and coworkers provided spectroscopic evidence for the involvement of a transient metal formyl intermediate in ethenediolate formation with an actinide complex.[31] The metal formyl was observed below −50 °C and not isolated. More recently, a number of main group and transition metal systems have been reported for ethenediolate formation,[40–44] in no case has a metal formyl intermediate been

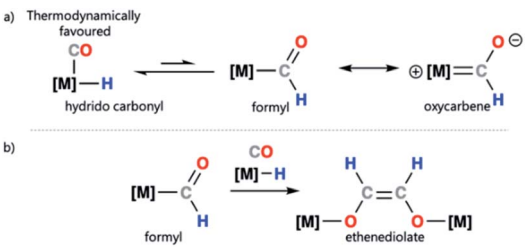

Scheme 1 (a) Transition metal–hydride to metal formyl equilibrium and canonical forms of a transition metal formyl complex; (b) proposed ethanediolate formation from a metal formyl complex.

Molecular Sciences Research Hub, Department of Chemistry, Imperial College London, 82 Wood Lane, White City, Shepherds Bush, London, W12 0BZ, UK. E-mail: m.crimmin@imperial.ac.uk

† Electronic supplementary information (ESI) available. CCDC 2116002–2116010. For ESI and crystallographic data in CIF or other electronic format see https://doi.org/10.1039/d2sc02063g

isolated, rather DFT calculations support their involvement in the mechanism for C–C bond formation.

In this study, we document the preparation, structural characterisation, and bonding analysis (NBO, ETS-NOCV, QTAIM) of a complete series of transition metal formyl complexes (M = Cr, Mn, Fe, Co, Rh, W, and Ir). This includes unprecedented examples of crystallographically characterised Cr, Co and Ir formyl complexes. Through reduction of a series of transition metal carbonyl complexes with a molecular magnesium hydride compound, the formyl ligand can be trapped as part of a chelating structure. Further reaction of a chromium formyl complex results in C–C bond formation and an ethenediolate species bridging the chromium and magnesium centres. DFT calculations are consistent with C–C bond formation occurring by stepwise process involving: (i) reduction of the metal formyl to generate an oxymethylene intermediate, (ii) insertion of CO, and (iii) a 1,2-hydride shift. This is an exceedingly rare example in which a well-defined transition metal formyl complex has been shown to be involved in a ethenediolate formation.[34]

Results and discussion

Synthesis and characterisation of metal formyl complexes

Reaction of a magnesium hydride dimer[45] (**1**) with a series of transition metal carbonyl complexes (**2**) in toluene solution furnished the corresponding heterometallic formyl complexes (**3**) in 21–68% isolated yields (Scheme 2). These reactions occurred readily at 22 °C as evidenced through a marked colour changes and diagnostic spectroscopic data. In C_6D_6 solution, the transition metal formyl species **3a–h** were characterized by singlet resonances between δ_H = 13.05–15.11 ppm and δ_C = 240–310 ppm in the ^{1}H and $^{13}C\{^1H\}$ NMR spectra respectively. Direct connection between the C and H atoms of the M–CHO fragment was confirmed by heteronuclear single quantum coherence (HSQC) NMR experiments. Further coupling was apparent in cases of spin active transition metals; the formyl ligand of **3b** shows $^2J_{W-H}$ = 9.0 Hz, while **3g** shows $^2J_{Rh-H}$ = 2.1 Hz and $^1J_{Rh-C}$ = 56.0 Hz. Bridging magnesium hydride resonances ranged δ_H = 2.86–3.17 ppm in the ^{1}H NMR spectra, upfield of the bridging hydride in **1** (δ_H = 4.02 ppm). No trend between transition metal fragment and hydride resonance was observed.

The infrared data for complexes **3a–h** show characteristic stretching frequencies for both the isocarbonyl and carbonyl ligands (Table S3 and Fig. S13–S21†). Terminal carbonyl ligands on **3a–e** displayed stretching frequencies at 1916–2067 cm^{-1}. **3f–h** showed no stretches in this region. The isocarbonyl ligands bridging the magnesium to transition metal centre appear as strong intensity bands at 1674–1791 cm^{-1}. Typical formyl stretches appear at a medium intensity in the range 1530–1630 cm^{-1}, red-shifted from the carbonyl ligands.[46,47]

Complexes **3a–h** show stretching frequencies at 1513–1520 cm^{-1}, with the ν(CO) stretch for the M–CHO fragment potentially masked by the C=N stretch of the β-diketiminate ligand. Formyl ligand C–H bonds are observed as a weak intensity stretching frequency at 2546–2635 cm^{-1} for **3a**, **3b**, **3d**, and **3f–h**; formyl C–H stretches in **3c** and **3e** were not observed.

All eight members of the series (**3a–h**) have been characterised in the solid state by single crystal X-ray diffraction analysis (Fig. 1 and Table 1). In all cases these structures showed a key motif involving an 8-membered ring comprised of the transition metal and two magnesium sites, along with the formyl, isocarbonyl and hydride ligands. While all complexes demonstrate the same structural type, only in **3c** and **3f** is the structure free from disorder, in the other cases positional disorder between the isocarbonyl and formyl sites of the ring is observed.

Complex **3c**, a representative example, crystallises in the $P\bar{1}$ space group, with the five carbon ligands arranged in a trigonal bipyramidal geometry around the iron centre. The formyl ligand occupies the axial position with a Mg–H–Mg bridge to a *cis* equatorial carbonyl ligand. The iron–carbon formyl bond of 1.935(9) Å is markedly longer than the average metal–carbon bonds to the carbonyl ligands 1.81(1) Å.

Within the series **3a–h**, M–C bond lengths to the formyl ligand range 1.80(3)–2.19(2) Å. The longest M–C bond lengths are recorded for the most electron deficient d^6 transition metal fragments (**3a** and **3b**), while some of the shortest M–C distances are recorded for the most electron rich d^8 transition metal fragments (**3f–h**). The disorder inherent in these structures results in large estimated standard deviations on the data, but they are also reproduced by Density Functional Theory (DFT) calculations. In most cases, the hydride ligand could be located within the Fourier difference map, while the location of this atom should be treated with caution, the Mg–H–Mg bond angles varied 146(1)–160(3)°. This angle is obtuse, presumably to achieve the geometry for the bimetallic magnesium fragment to bridge two mutually *cis* sites of the transition metal.

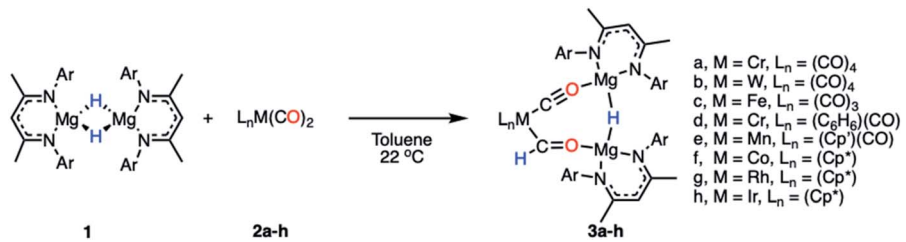

1 2a-h 3a-h

Scheme 2 Synthetic procedure for the formation of compounds **3a–h** (Ar = 2,6-diisopropylphenyl, Cp′ = methylcyclopentadienyl, Cp* = pentamethylcyclopentadienyl).

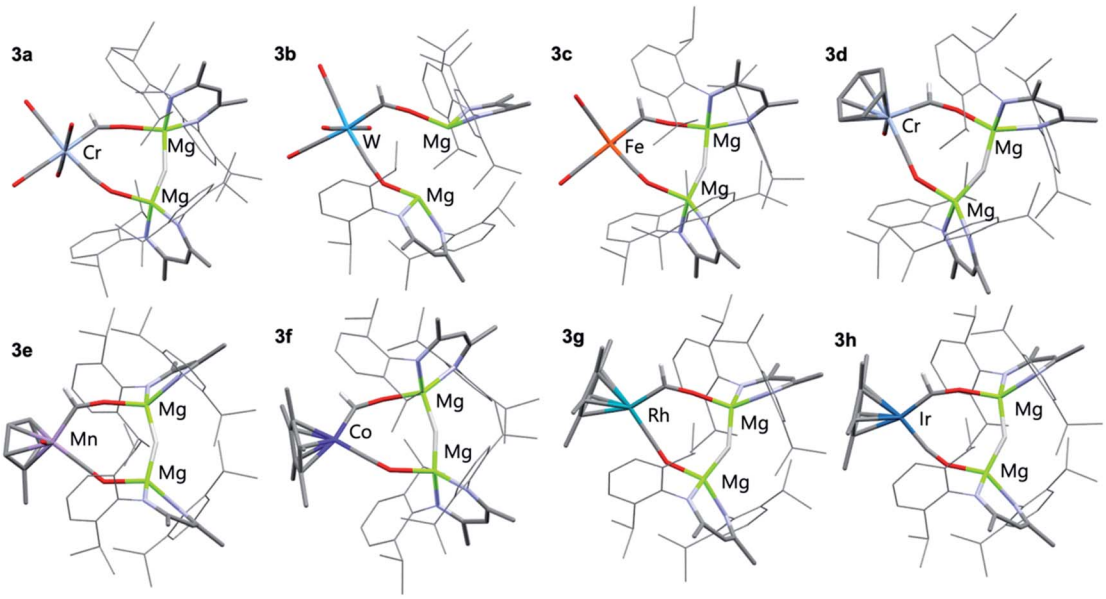

Fig. 1 X-ray crystal structures of **3a–h**. Solvent molecules and most hydrogen atoms removed for clarity.

Electronic structure

The electronic structure and bonding interaction between the formyl ligand and transition metal centre were investigated using DFT. Calculations were performed in Gaussian 09 and Orca 4.2.1. Natural Bonding Orbital (NBO) and Extended Transition State-Natural Orbital Chemical Valence (ETS-NOCV) methods were employed to interrogate the bonding interactions in **3a–h**. Structures were optimised using the wB97X-D functional, a hybrid basis set was used 6-31G** (C, H), 6-311+G* (N, O) while the SDDAll pseudopotential and associated basis sets were used to describe Mg and M centres.[48–53]

NBO calculations were performed on complexes **3a–h**. Analysis of the Natural Population Analysis (NPA) charges suggests that the binding interaction between the transition metal fragment and dimagnesium hydride fragment is largely ionic. The hydride (−0.8) and oxygen atoms (−0.9) directly attached to magnesium bear significant negative charge while these magnesium sites themselves are highly electropositive (+1.8). Comparison of data for **3a** and **3b** to the theoretical models $[M(CO)_5(CHO)]^-$ (M = Cr, Mo, W) shows little change in the NPA charges, supporting the idea that there is a large ionic contribution to the bonding between the transition metal and main group fragments. QTAIM calculations point to the same conclusion, with hydride (−0.8), oxygen (−1.4) and magnesium (+1.8) charges complimenting the NBO data (Tables S5, S6 and S9†).

Comparison of both the NPA charges and Wiberg bond indices (WBI) for selected sets of complexes within the series allows the influence of d^n electron count, ligand, and transition metal on the bonding to be speculated upon (Table 2). The trends in the calculated data are such that only a course comparison can be made, however comparing examples based on electron-deficient group 6 and 8 metal fragments (*e.g.* **3a–c**) with more electron-rich group 9 metals (*e.g.* **3f–h**) suggests that the oxycarbene character increases with increasing electron-density on the metal. This proposed trend is manifest in higher M–C WBIs, lower C–O WBIs, decreased charge on M, and increased charge on O for the more-electron rich members of the series.

ETS-NOCV calculations were performed on complexes **3a–h** to obtain quantitative data on the nature and strength of the

Table 1 Selected structural parameters for M–CHO components for complexes **3**

	M–C (XRD)[a] (Å)	M–C (DFT)[b] (Å)	C–O (XRD)[a] (Å)	C–O (DFT)[b] (Å)	M–C–O (XRD) (°)
3a	2.054(9)	2.048	1.210(7)	1.254	132.0(6)
3b	2.19(2)	2.200	1.26(2)	1.251	130(1)
3c	1.935(9)	1.934	1.221(2)	1.247	128.5(6)
3d	1.95(1)	1.943	1.234(9)	1.263	137.1(8)
3e	1.91(2)	1.903	1.24(1)	1.253	133(1)
3f	1.804(8)	1.816	1.255(9)	1.262	135.9(6)
3g	1.920(6)	1.932	1.270(5)	1.255	134.0(5)
3h	1.80(3)	1.935	1.27(3)	1.260	151(3)

[a] Average bond length, provided with pooled estimated standard deviation (ESDs) in parentheses where possible. [b] Calculated bond length.

Table 2 Select Natural Population Analysis (NPA) charges and Wiberg Bond Indices (WBI) for complexes **3a–h**. Complete NBO data can be found in the ESI (Tables S5 and S6)

	NPA charge					WBI		
	M	C	O	Mg	H	M–C	C–O	O–Mg
3a	−1.29	0.27	−0.86	1.78	−0.80	0.55	1.52	0.052
3b	−0.86	0.19	−0.86	1.76	−0.80	0.60	1.53	0.054
3c	−0.46	0.25	−0.85	1.77	−0.80	0.57	1.52	0.055
3d	−0.66	0.30	−0.91	1.77	−0.80	0.87	1.44	0.057
3e	−0.42	0.31	−0.87	1.77	−0.80	0.77	1.50	0.06
3f	0.21	0.21	−0.91	1.77	−0.79	0.79	1.42	0.06
3g	0.17	0.23	−0.89	1.77	−0.79	0.85	1.44	0.058
3h	0.28	0.18	−0.90	1.77	−0.79	0.95	1.40	0.058

metal–ligand interaction (Tables S7 and S8†). Before embarking on this analysis, it is useful to consider the frontier molecular orbitals of a bent $\{CHO\}^-$ triatomic; the HOMO shows significant carbon based lone-pair character, while the LUMO is a π^* orbital with the largest coefficient on the carbon atom (Fig. S31†). In all cases for **3a–h** the principal contribution ($\nabla\rho_1$) to the bonding interaction is the σ-donation of the HOMO of the $\{CHO\}^-$ ligand to a transition-metal d-orbital. The secondary ($\nabla\rho_2$) and tertiary ($\nabla\rho_3$) interactions involve π back-donation from a metal-based orbital to the orthogonal π^*-orbitals of the $\{CHO\}^-$ ligand.‡

These donor–acceptor interactions can be visualised in the deformation density plots (Fig. 2b and Tables S11–S13†). The total orbital interaction between the formyl ligand and transition metal fragment, ΔE_{orb}, broadly increases across the first-row transition metals (**3a** *vs.* **3e**; **3d** *vs.* **3f**) and down the triad (**3f** *vs.* **3g** *vs.* **3h**). Data that could again be interpreted in terms of increased oxycarbene character increasing the strength of the bonding interaction with more electron-rich transition metal fragments.§

Solution stability and ethenediolate formation

To further assess their stability in solution, half-lives for complexes of **3a–h** in C_6D_6 at 22 °C have been measured (Table S4 and Fig. S22–S30†). In all cases kinetics followed a first-order decay, consistent with an intramolecular pathway: **3a** ($t_{1/2}$ = 2 h), **3b** ($t_{1/2}$ = 2 h), **3c** ($t_{1/2}$ = 57 h), **3d** ($t_{1/2}$ = 136 h), **3e** ($t_{1/2}$ = 224 h), **3f** ($t_{1/2}$ = 330 h), **3g** ($t_{1/2}$ = 217 h), **3h** ($t_{1/2}$ = 533 h). The most stable complexes in this series **3d–h** are those which contain electron-rich and sterically demanding ligands on the transition metal fragment. It has been previously suggested that transition metal formyl complexes can be stabilised by inclusion of a sterically demanding ligand, commonly a bulky phosphine.[3,4,30,54,55] The half-life for complex **3a** ($t_{1/2}$ = 2 h), was identical in C_6D_6 and THF solvent and did not change when running the reaction under 1 atm. of CO. These results suggest that neither the solvent nor the concentration of CO in solution influences the stability of the formyl ligand.

Onward reaction of **3a** yielded a single well-defined product **4a** (Scheme 3). **4a** can be synthesised *via* three routes: thermolysis of **3a**, reaction of **3a** with 0.5 equiv. of **1**, and direct 1 : 1 reaction of **1** with **2a** overnight; yields ranged 62–70% (NMR), 31–51% (isolated crystals). **4a** has been characterised by multinuclear NMR spectroscopy and single crystal X-ray diffraction (Fig. 3). The CO coupling pathway involving a well-defined formyl intermediate stands in stark contrast to the expected α-elimination reaction. **4a** comprises an ethenediolate $\{C_2H_2O_2\}^{2-}$ unit bridging chromium and magnesium centres.

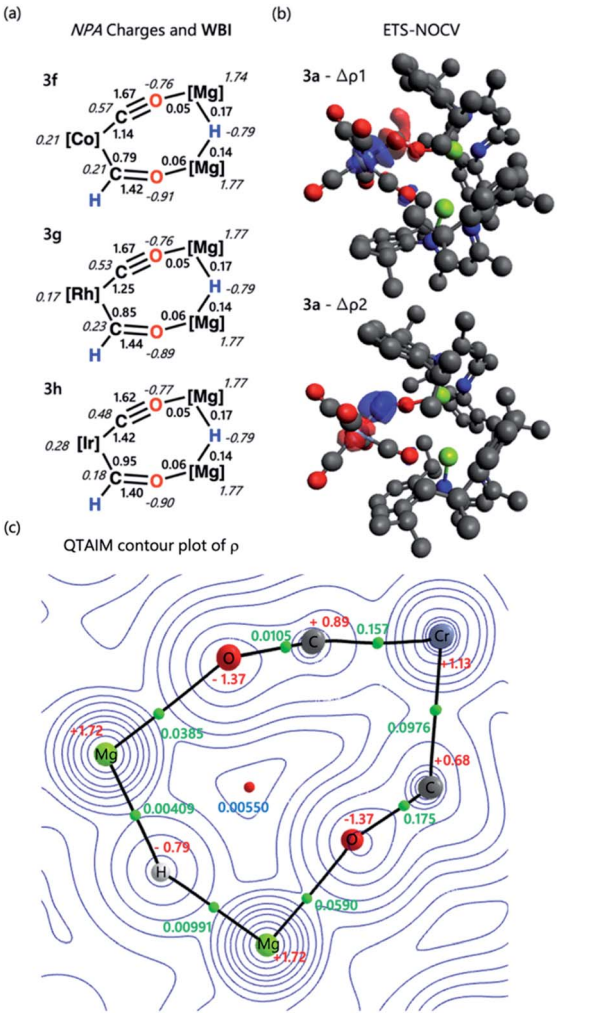

Fig. 2 (a) Select NPA charges and Wiberg bond indices for complexes **3f–h**; (b) select ETS-NOCV deformation density data for complex **3a**. Charge flow is from red to blue; (c) QTAIM contour plot of ρ for **3a**. Charges are depicted in red, electron density at the bond critical point (ρ) in green, and ring critical point in blue. Complete NBO, ETS-NOCV, and QTAIM data can be found in the ESI.†

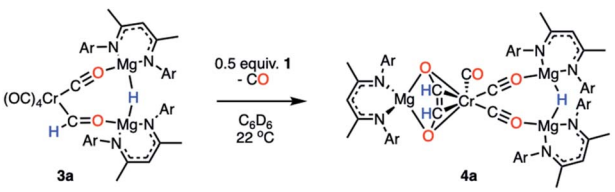

Scheme 3 Transformation of **3a** to **4a**, a C–C coupled product.

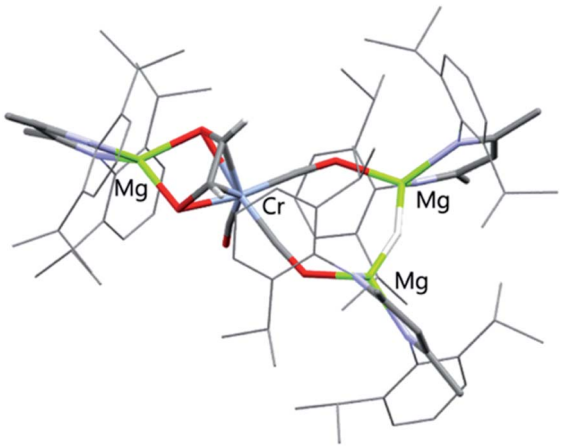

Fig. 3 X-ray crystal structures of **4a**. Solvent molecules and most hydrogen atoms removed for clarity.

From the perspective of chromium, the new ligand is reminiscent of a 6-electron (2p + 2 oxygen LP) analogue of a butadiene motif.

In solution, HSQC experiments on **4a** led to the assignment of the ethenediolate protons as two singlet resonances at δ_H = 4.33 (1H) and 5.45 ppm (1H), associated carbon resonances occur at δ_C = 110.2 and 110.5 ppm. The spectroscopic data are consistent with that reported for related magnesium ethenediolate complexes by Hill and Jones.[43,44] The hydride bridging the two magnesium centres appears as a singlet resonance at δ_H = 2.72 ppm. In the solid state, the key ethenediolate ligand spans chromium and magnesium centre. Respective C=C and C–Cr bond lengths of 1.369(5) and 2.104(3)–2.109(3) Å indicate an ligand binding in a η^4-fashion to the central chromium atom. The $\{C_2H_2O_2\}^{2-}$ unit coordinates through oxygen to a magnesium centre with Mg–O bond lengths of 1.986(2) and 1.992(2) Å.

DFT calculations were used to investigate ethenediolate formation from a formyl intermediate. Calculations were performed on a model system comprised of $[Cr(CO)_5(CHO)]^-$ and monomeric **1**. Such a simplification is necessary for computational cost, however this system still provides insight into the most likely steps involved in the mechanism for C–C bond formation. The overall formation of the ethenediolate from the chromium formyl complex is exergonic with $\Delta G^\circ_{rxn}(298\ K) = -37.1$ kcal mol^{-1}. The most plausible pathway calculated for ethenediolate formation follows that originally postulated by Bercaw and co-workers (Fig. 4).[37] Importantly, our work now connects a well-defined and structurally characterised formyl intermediate to an ethenediolate product.

The stepwise mechanism is initiated by the coordination of **1** to the oxygen atom of the formyl ligand of $[Cr(CO)_5(CHO)]^-$ to give **Int-1**. **Int-1** undergoes hydride-transfer from Mg to Cr–CHO *via* **TS-1** ($\Delta G^\ddagger$ = 19.7 kcal mol^{-1}), forming **Int-2**. This step is formally a hydromagnesiation of the transition metal formyl and generates a new oxymethylene ligand. From **Int-2**, C–C coupling proceeds through a migratory insertion reaction that is characterised by a low energy transition state **TS-2** ($\Delta G^\ddagger$ =

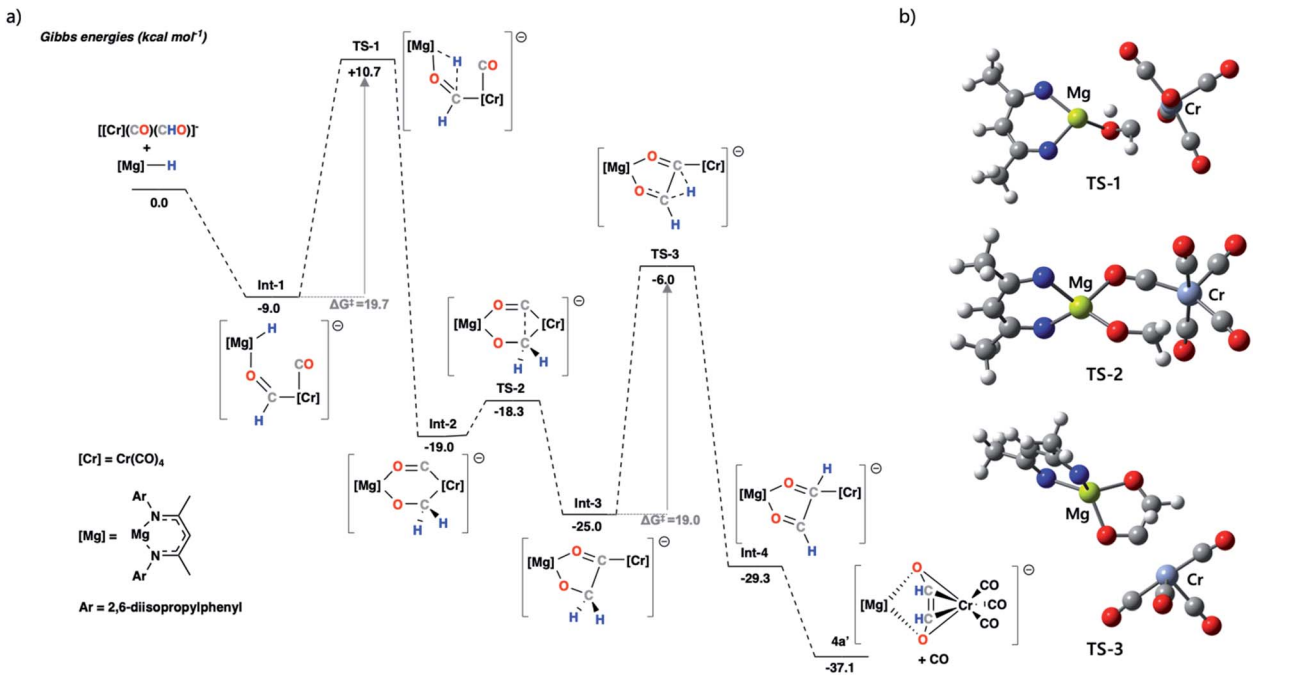

Fig. 4 (a) Calculated potential energy surface for ethenediolate formation from a model chromium formyl anion. The structures were optimised using the ωB97X-D functional, a hybrid basis set was used 6-31G** (C, H), 6-311+G* (N, O) while the SDDAll pseudopotential and associated basis sets were used to describe Mg and Cr centres. Solvent corrections were applied *via* single point corrections, using the PCM (solvent = toluene) model; (b) optimised geometry structures for transition states **TS-1**, **TS-2** and **TS-3**; 2,6-diisopropylphenyl and most hydrogen atoms removed for clarity (carbon = grey, chromium = teal, hydrogen = white, magnesium = yellow, nitrogen = blue, oxygen = red).

0.7 kcal mol^{-1}). **TS-2** proceeds to a five-coordinate chromium complex **Int-3**. **Int-3** can then undergo a 1,2-H shift *via* **TS-3** ($\Delta G^{\ddagger}$ = 19.0 kcal mol^{-1}) to form the ethenediolate ligand which at this point is coordinated to chromium in an η^1-fashion. Subsequent dissociation of CO gives the product **4a′** and occurs with translation of the ethenediolate to an η^4-mode.

NBO analysis was performed on the key transition states on the pathway. Analysis of the hydromagnesiation step shows an increased positive charge on the H atom as it moves from Mg in **Int-1** (−0.72) toward C in **TS-1** (−0.51). At the same time there is an expected decrease in the WBI for the Mg–H bond (0.40 to 0.15; **Int-1** to **TS1**). The 1,2-H atom shift occurs with re-organisation of the electron density in the $\{C_2H_2O_2\}^{2-}$ fragment. Most notably, from **Int-3** to **TS3** the C–C bond WBI increases from 0.95 to 1.24 as the ethenediolate forms (Fig. S43†). Alternative mechanistic pathways gave considerably higher energy barriers or did not proceed towards the known ethenediolate product (Fig. S44†). For example, the direct hydromagnesiation of a carbonyl ligand of $[Cr(CO)_5(CHO)]^-$ with **1** to form a bis(formyl) intermediate was found to proceed by activation barrier of over 50 kcal mol^{-1}, effectively ruling out this pathway.

Conclusions

In summary, we report the first comprehensive series of transition-metal formyl complexes (M = Cr, Mn, Fe, Co, Rh, W, Ir). These include unprecedented examples of crystallographically characterised Cr, Co and Ir formyl complexes. In all cases, the metal bound formyl ligand is stabilised by a heterometallic effect. We investigated this oxycarbene electronic structure through a series of density functional theory calculations (NBO, ETS-NOCV, QTAIM), and concluded that more electron rich metal centres likely result in more oxycarbene character, and thus stabilisation of the metal-formyl ligand. Remarkably, onwards reaction of a chromium formyl complex yields C–C coupling and an isolable ethenediolate complex. This serves as the first direct example of carbon–carbon bond formation at a well-defined and isolable metal-formyl complex.

Data availability

Experimental procedures, details of the calculations, and additional data can be found in the ESI† (.pdf). X-ray data is available in .cif format.

Author contributions

JMP conducted all experimental and computational work. AJPW and JMP solved and refined single crystal XRD data. All authors contributed to writing the manuscript.

Conflicts of interest

There are no conflicts to declare.

Acknowledgements

We thank Imperial College London for the award of a Schrödinger's Scholarship (JMP). Dr Andreas Phanopoulos is thanked for insightful discussions. Dr Olga Ekkert is thanked for running preliminary experiments on this project. We also thank the EPSRC for funding (EP/S036628/1).

Notes and references

‡ For Ir, further splitting of the metal-based d-orbitals (due to overlap with ligand SALCs of CO) results in both ρ_1 and ρ_2 interactions being σ-donation from the HOMO of $\{CHO\}^-$ to empty orbitals on the Ir fragment. ρ_3 is π-backdonation.

§ While the treatment allows analysis of the key bonding interaction between the formyl ligand and the transition metal, it does not lead to the lowest total orbital interaction energies ΔE_{ORB}. A second set of ETS-NOCV calculations split complexes **3** into anionic and cationic fragments by dividing at the Mg–O bond, giving consistently lower ΔE_{ORB} values (Table S8 and Fig. S34†).

1 N. M. West, A. J. M. Miller, J. A. Labinger and J. E. Bercaw, *Coord. Chem. Rev.*, 2011, **255**, 881–898.
2 C. P. Casey and S. M. Neumann, *J. Am. Chem. Soc.*, 1976, **98**, 5395–5396.
3 W. Tam, W.-K. Wong and J. A. Gladysz, *J. Am. Chem. Soc.*, 1979, **101**, 1589–1591.
4 H. Berke and G. Weiler, *Angew. Chem., Int. Ed.*, 1982, **21**, 150–151.
5 M. D. Farnos, B. A. Woods and B. B. Wayland, *J. Am. Chem. Soc.*, 1986, **108**, 3659–3663.
6 A. R. Cutler, P. K. Hanna and J. C. Vites, *Chem. Rev.*, 1988, **88**, 1363–1403.
7 B. H. Davis and M. L. Occelli, *Advances in Fischer–Tropsch Synthesis, Catalysts, and Catalysis*, 2020.
8 J. A. Labinger, *J. Organomet. Chem.*, 2017, **847**, 4–12.
9 D. Unruh, K. Pabst and G. Schaub, *Energy Fuels*, 2010, **24**, 2634–2641.
10 O. R. Inderwildi, S. J. Jenkins and D. A. King, *Angew. Chem., Int. Ed.*, 2008, **47**, 5253–5255.
11 S. Srinivas, R. K. Malik and S. M. Mahajani, *Energy Sustainable Dev.*, 2007, **11**, 66–71.
12 A. J. Ragauskas, C. K. Williams, B. H. Davison, G. Britovsek, J. Cairney, C. A. Eckert, W. J. Frederick, J. P. Hallett, D. J. Leak, C. L. Liotta, J. R. Mielenz, R. Murphy, R. Templer and T. Tschaplinski, *Science*, 2006, **311**, 484–489.
13 J. P. Collman and S. R. Winter, *J. Am. Chem. Soc.*, 1973, **95**, 4089–4090.
14 T. J. Collins and W. R. Roper, *J. Chem. Soc., Chem. Commun.*, 1976, **24**, 1044–1045.
15 J. A. Gladysz, G. M. Williams, W. Tam and D. L. Johnson, *J. Organomet. Chem.*, 1977, **140**, C1–C6.
16 R. L. Pruett, R. C. Schoening, J. L. Vidal and R. A. Fiato, *J. Organomet. Chem.*, 1979, **182**, 57–60.
17 C. P. Casey, S. M. Neumann, M. A. Andrews and R. McAlister Donald, *Pure Appl. Chem.*, 1980, **52**, 625–633.
18 B. A. Narayanan, C. A. Amatore and J. K. Kochi, *Organometallics*, 1984, **3**, 802–804.
19 G. Nelson and C. E. Sumner, *Organometallics*, 1986, **5**, 1983–1990.

20 P. A. Kongshaug and R. G. Miller, *Organometallics*, 1987, **6**, 372–378.
21 M. G. Richmond and J. K. Kochi, *Organometallics*, 1987, **6**, 777–788.
22 M. G. Richmond and J. K. Kochi, *J. Organomet. Chem.*, 1987, **323**, 219–232.
23 P. Leoni, A. Landi and M. Pasquali, *J. Organomet. Chem.*, 1987, **321**, 365–369.
24 J. A. Partin and M. G. Richmond, *J. Organomet. Chem.*, 1988, **353**, 13–16.
25 A. Asdar, C. Lapinte and L. Toupet, *Organometallics*, 1989, **8**, 2708–2717.
26 H. Berke and R. Hoffmann, *J. Am. Chem. Soc.*, 1978, **100**, 7224–7236.
27 S. L. Van Voorhees and B. B. Wayland, *Organometallics*, 1987, **6**, 204–206.
28 K. R. Lane and R. R. Squires, *Polyhedron*, 1988, **7**, 1609–1618.
29 G. Pacchioni, P. Fantucci, J. Koutecký and V. Ponec, *J. Catal.*, 1988, **112**, 34–43.
30 J. S. Sapsford, S. J. Gates, L. R. Doyle, R. A. Taylor, S. Díez-González and A. E. Ashley, *Inorg. Chim. Acta.*, 2019, **488**, 201–207.
31 P. J. Fagan, K. G. Moloy and T. J. Marks, *J. Am. Chem. Soc.*, 1981, **103**, 6959–6962.
32 P. T. Wolczanski, R. S. Threlkel and J. E. Bercaw, *J. Am. Chem. Soc.*, 1979, **101**, 218–220.
33 P. R. Elowe, N. M. West, J. A. Labinger and J. E. Bercaw, *Organometallics*, 2009, **28**, 6218–6227.
34 P. T. Barger, B. D. Santarsiero, J. Armantrout and J. E. Bercaw, *J. Am. Chem. Soc.*, 1984, **106**, 5178–5186.
35 D. A. Katahlra, K. G. Moloy and T. J. Marks, *Organometallics*, 1982, **1**, 1723–1726.
36 E. L. Werkema, L. Maron, O. Eisenstein and R. A. Andersen, *J. Am. Chem. Soc.*, 2007, **129**, 2529–2541.
37 J. M. Manriquez, R. McAlister Donald, R. D. Sanner and J. E. Bercaw, *J. Am. Chem. Soc.*, 1976, **98**, 6733–6735.
38 J. M. Manriquez, D. R. McAlister, R. D. Sanner and J. E. Bercaw, *J. Am. Chem. Soc.*, 1978, **100**, 2716–2724.
39 P. T. Wolczanski and J. E. Bercaw, *Acc. Chem. Res.*, 1980, **13**, 121–127.
40 C. C. Cummins, G. D. Van Duyne, C. P. Schaller and P. T. Wolczanski, *Organometallics*, 1991, **10**, 164–170.
41 W. J. Evans, J. W. Grate and R. J. Doedens, *J. Am. Chem. Soc.*, 1985, **107**, 1671–1679.
42 G. M. Ferrence, R. McDonald and J. Takats, *Angew. Chem., Int. Ed.*, 1999, **38**, 2233–2237.
43 R. Lalrempuia, C. E. Kefalidis, S. J. Bonyhady, B. Schwarze, L. Maron, A. Stasch and C. Jones, *J. Am. Chem. Soc.*, 2015, **137**, 8944–8947.
44 M. D. Anker, M. S. Hill, J. P. Lowe and M. F. Mahon, *Angew. Chem., Int. Ed.*, 2015, **127**, 10147–10149.
45 S. P. Green, C. Jones and A. Stasch, *Angew. Chem., Int. Ed.*, 2008, **120**, 9219–9223.
46 F. G. A. Stone, R. West and J. A. Gladysz, *Adv. Organomet. Chem.*, 1982, **20**, 1–35.
47 R. M. Silverstein, G. C. Bassler and T. C. Morrill, *Spectrometric Identification of Organic Compounds*, 3rd edn, 1974.
48 M. Garçon, N. W. Mun, A. J. P. White and M. R. Crimmin, *Angew. Chem., Int. Ed.*, 2021, **60**, 6145–6153.
49 M. Garçon, C. Bakewell, G. A. Sackman, A. J. P. White, R. I. Cooper, A. J. Edwards and M. R. Crimmin, *Nature*, 2019, **574**, 390–393.
50 M. J. Butler, A. J. P. White and M. R. Crimmin, *Angew. Chem., Int. Ed.*, 2016, **55**, 6951–6953.
51 A. Hicken, A. J. P. White and M. R. Crimmin, *Angew. Chem., Int. Ed.*, 2017, **56**, 15127–15130.
52 J. Da Chai and M. Head-Gordon, *Phys. Chem. Chem. Phys.*, 2008, **10**, 6615–6620.
53 J. Da Chai and M. Head-Gordon, *J. Chem. Phys.*, 2008, **128**, 084106.
54 S. G. Davies and A. J. Smallridge, *J. Organomet. Chem.*, 1990, **397**, 13–19.
55 B. H. Berke, G. Huttner, O. Scheidsteger and G. Weiler, *Angew. Chem., Int. Ed.*, 1984, **23**, 735–736.